Variational Monte Carlo Analysis of Hydrogen and the Hydrogen Molecule

Gavin Xie 02410400

***Abstract*—This project applies Variational Monte Carlo (VMC) methods to compute the ground-state energies of hydrogenic systems and to determine the molecular potential of H_2. A three-parameter variational ansatz is used to evaluate the H_2 ground-state energy at different internuclear separations, and the resulting energy curve is fitted to a Morse potential using chi-square minimization. The fitted parameters, $r_0 = 1.404 \pm 0.001$ bohr, $D = 0.1425 \pm 0.0003$ Hartree, and $a = 1.136 \pm 0.005$ bohr^{-1}, yield an equilibrium bond length consistent with known values and a physically reasonable dissociation energy.**

I. Introduction

THIS project investigates the ground-state energy of the hydrogen molecule using Variational Monte Carlo (VMC). Numerical differentiation and Metropolis sampling methods are first validated on the one-dimensional harmonic oscillator before a parametrized ansatz is introduced to obtain the ground-state wavefunction by minimizing the Hamiltonian expectation. These techniques are then extended to the hydrogen atom and subsequently to the hydrogen molecule, where optimized ground-state energies at various internuclear separations are used to extract the bond length and dissociation energy. A chi-square procedure is finally applied to fit the resulting energy curve to a Morse potential.

II. Theory

A. Justification of Monte Carlo integration

The expectation value of the Hamiltonian is evaluated using Monte Carlo integration, a method well suited to quantum systems whose configuration space scales as $3N$ dimensions for N electrons. Deterministic quadrature schemes, such as Newton–Cotes rules, become infeasible in this regime because the number of grid points grows exponentially with dimension, and they further require smooth, grid-aligned integrands—conditions violated by electronic wavefunctions, which contain sharp features such as nuclear cusps.

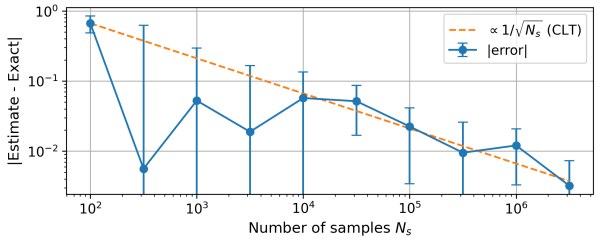

Fig. 1: Convergence of the Monte Carlo estimator for the test integral of $f(x) = x^2e^{-x}$ under $\rho(x) = e^{-x}$. The absolute error decreases proportionally to $N_s^{-1/2}$, consistent with the central limit theorem.

Monte Carlo integration avoids these limitations and provides several advantages. Its convergence rate, $\mathcal{O}(N_s^{-1/2})$ for N_s samples, is independent of dimensionality, making it effective for high-dimensional systems. Sampling directly from the probability density $\rho(\mathbf{R})$ focuses computational effort where the wavefunction has significant weight, eliminating wasted evaluations in regions of negligible contribution. Equation (1) given in the note can be written as [1]

$$\langle H \rangle = \int d\mathbf{R}\, \rho(\mathbf{R})\, \frac{\hat{H}\, \Psi_T(\mathbf{R})}{\Psi_T(\mathbf{R})} = \mathbb{E}_\rho[E_l(\mathbf{R})] \quad (1)$$

where the local energy is

$$E_l(\mathbf{R}) = \frac{\hat{H}\Psi_T(\mathbf{R})}{\Psi_T(\mathbf{R})}. \quad (2)$$

Using N_s independent samples $\mathbf{R}^{(i)} \sim \rho(\mathbf{R})$, the Monte Carlo estimator of the expectation value is

$$\langle H \rangle \approx \frac{1}{N_s} \sum_{i=1}^{N_s} E_l\big(\mathbf{R}^{(i)}\big)\,, \quad (3)$$

By the central limit theorem, $\langle H \rangle$ converges to the exact variational energy as $N_s \to \infty$. To verify this convergence behaviour explicitly, I compare the Monte Carlo estimate of the integral of the test function $f(x) = x^2e^{-x}$ under the sampling

distribution $\rho(x) = e^{-x}$ against its analytical value for increasing sample sizes. The results are shown in Fig. 1.

B. Minimization Methods

Two minimization strategies are employed in this project. For single-parameter problems—such as optimizing the Metropolis step size δ in 1D, 3D, and 6D sampling, determining the hydrogen ground-state eigenfunction, or performing χ^2 fitting for the Morse potential—gradient descent is used due to its simplicity and reliability in low-dimensional settings. However, it becomes inefficient for multi-parameter optimization. In the H_2 case, where the wavefunction depends on three variational parameters $\boldsymbol{\theta}$, Monte Carlo noise causes gradient descent to converge slowly and inconsistently. For this reason, a Quasi-Newton method is adopted for the multi-parameter minimization. With proper tuning, it typically converges in about six iterations, compared with more than fifty for gradient descent, providing a substantial reduction in computational cost despite its higher per-step complexity.

The gradient-descent implementation was first validated using the test function $f(x) = (x-1)^2$ with a learning rate of 0.01 and a gradient tolerance of 10^{-6}. Under these settings, the algorithm converged to the analytic minimum at $x = 1$, reaching $x = 1 + 5 \times 10^{-7}$ after 700 iterations. The Quasi-Newton method was validated using

$$f(x, y, z) = (x-1)^2 + 2(y-1)^2 + 3(z-1)^2,$$

which has a known minimum of $f(1, 1, 1) = 0$. Using a gradient tolerance of 10^{-6}, the method converged in 8 iterations and returned $\mathbf{x}_{\min} = (1 - 1 \times 10^{-8}, 1 - 1 \times 10^{-8}, 1 + 1 \times 10^{-8})$ with $f(\mathbf{x}_{\min}) = 2 \times 10^{-16}$, demonstrating accurate and efficient convergence.

For the hydrogen molecule, the Quasi-Newton method must account for Monte Carlo noise in the energy evaluations. To determine when the optimization has reached the noise floor [2], the change in energy between successive iterations, $\Delta E = E_k - E_{k-1}$, is compared with its statistical uncertainty,

$$\sigma_{\Delta E} = \sqrt{\sigma_k^2 + \sigma_{k-1}^2}, \tag{4}$$

assuming independent Monte Carlo estimates. Convergence is declared when $|\Delta E| < c_\sigma \, \sigma_{\Delta E}$ for a chosen threshold c_σ after a minimum number of iterations, ensuring that further updates would be smaller than intrinsic Monte Carlo fluctuations and that the optimization has reached its noise-limited accuracy.

C. Metropolis sampling

The Metropolis–Hastings algorithm constructs a Markov chain whose stationary distribution is the target density $\rho(x) = |\psi_n(x)|^2$ [1]. Starting from an initial point, trial moves are generated by adding a random displacement drawn from a symmetric proposal distribution, typically a zero-mean unit-variance Gaussian [3]. The proposal width δ controls the exploration scale and is tuned for sampling efficiency. Each proposed move is accepted according to the Metropolis rule based on the ratio of target densities; otherwise, the chain remains at its current state. After discarding burn-in, the resulting samples follow $\rho(x)$, albeit with the usual Markov-chain correlations [3].

The advantages of Metropolis sampling become evident when compared with alternative methods. Transformation and rejection sampling produce independent samples, but transformation sampling requires an analytically invertible cumulative distribution, which is rarely available for realistic quantum systems, while rejection sampling depends on a suitable envelope function, which is difficult to construct efficiently for structured wavefunctions such as that of H_2 [4]. In contrast, Metropolis sampling requires only the evaluation of $|\psi_n(x)|^2$ up to a normalization constant, making it well suited to variational Monte Carlo. Its primary limitations are the presence of autocorrelations and the need to tune the proposal width δ.

Figure 2 demonstrates good agreement between the Metropolis-sampled distributions and the analytical Gaussians in both one and three dimensions, providing confidence that the sampler has been implemented correctly.

D. Metropolis Step Size Optimization

In Metropolis sampling, the proposal step size δ strongly influences the statistical efficiency of the Markov chain by affecting the integrated autocorrelation time τ_{int} and thus the effective sample size $N_{\text{eff}} \approx N/(2\tau_{\text{int}})$. Small values of δ yield high acceptance but slow exploration, whereas large values

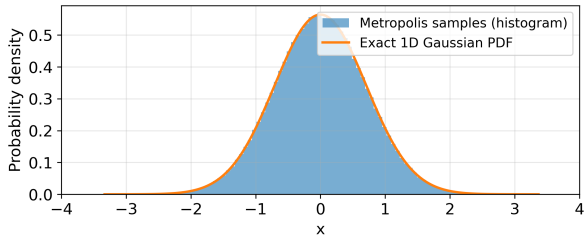

(a) Comparison between Metropolis-generated samples and the exact 1D Gaussian probability density.

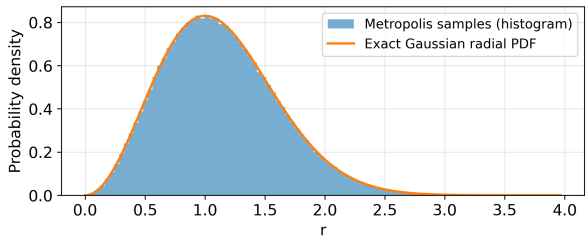

(b) Radial distribution obtained from 3D Metropolis sampling compared with the exact 3D Gaussian radial PDF.

Fig. 2: Validation of the Metropolis sampler using Gaussian test distributions.

are rarely accepted and cause the chain to stall. The integrated autocorrelation time is computed as [3]

$$\tau_{\text{int}} = \frac{1}{2} + \sum_{k=1}^{\infty} A(k), \tag{5}$$

where $A(k)$ is the autocorrelation function, evaluated here using the local energy E_l [3]. The sampling efficiency is quantified by

$$r = \frac{N_{\text{eff}}}{N}, \tag{6}$$

the statistical error of the Monte Carlo estimator by

$$\sigma_{\langle H \rangle} = \frac{\sigma_{\text{sample}}}{\sqrt{N_{\text{eff}}}}, \tag{7}$$

where σ_{sample} is the sample standard deviation. Accordingly, the optimal proposal width δ is obtained by applying a gradient-descent optimizer to maximize the efficiency rate r, a tuning strategy used throughout this project for all Metropolis samplers.

III. 1D Harmonic Oscillator

A. 1D Schrödinger Equation

The Schrodinger equation for a simple harmonic oscillator in 1D, and a single electron is given by [1]

$$-\frac{\hbar^2}{2m_e}\frac{d^2\psi(x)}{dx^2} + \frac{1}{2}m_e\omega^2 x^2\psi(x) = \mathcal{E}\,\psi(x) \tag{8}$$

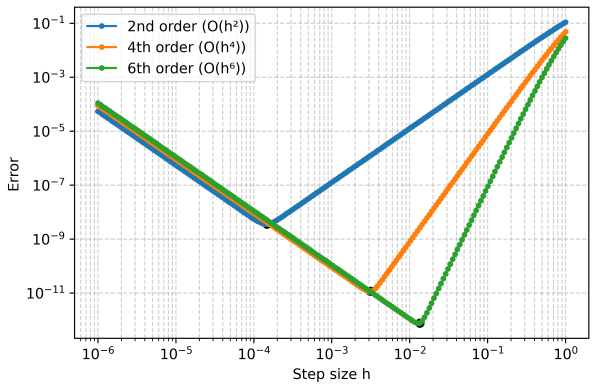

Fig. 3: Error of second-, fourth-, and sixth-order finite-difference Laplacians as a function of step size h. Each method exhibits the expected h^2, h^4, and h^6 scaling in the truncation-error regime, followed by loss of accuracy at small h due to floating-point roundoff.

where ψ is the wavefunction, $\mathcal{E}$ is the energy, m_e is the electron mass, $\hbar$ is the reduced Planck constant, and ω is the harmonic oscillator strength.

In Eq. 8 each term must have dimensions of an energy multiplied by the wavefunction. Dimensions of each variable and constant are shown in the Tab. I

Quantity	Symbol	Dimension
Wavefunction	$\psi(x)$	$L^{-1/2}$
Position	x	L
Mass	m_e	M
Reduced Planck constant	$\hbar$	ML^2T^{-1}
Angular frequency	ω	T^{-1}
Energy	$\mathcal{E}$	ML^2T^{-2}

TABLE I: Dimensions of all quantities and terms in the 1D harmonic oscillator Schrödinger equation.

B. 1D Finite Difference Method

To evaluate the effect of the finite-difference step size h, the local error was computed for several truncation orders. As shown in Fig. 3, the error decreases for moderate h but increases once h becomes too small, reflecting the trade-off between truncation and roundoff errors. The total error may be approximated as

$$\varepsilon(h) \sim h^{2m} + \frac{\epsilon_{\text{mach}}}{h^2}, \tag{9}$$

where the first term represents the truncation error of a $2m$-order central difference scheme, and the second term captures roundoff error arising from

floating-point cancellation. Here, ϵ_{mach} denotes machine precision.

Figure 3 shows clear minima for the second-, fourth-, and sixth-order schemes, with optimal values obtained via gradient-descent search and summarized in Table II.

Order	Optimal step size	Average error
2nd	$(1.55 \pm 0.2) \times 10^{-4}$	$(3.6 \pm 0.2) \times 10^{-9}$
4th	$(3.078 \pm 0.001) \times 10^{-3}$	$(1.148 \pm 0.6) \times 10^{-11}$
6th	$(1.174 \pm 0.001) \times 10^{-2}$	$(8.43 \pm 0.08) \times 10^{-13}$

TABLE II: Optimal step sizes h_{opt} and corresponding average errors for the 2nd-, 4th-, and 6th-order finite-difference approximations of the second derivative. Uncertainties represent the standard deviation obtained from plateau sampling of the minimisation algorithm.

Table II shows that the fourth–order finite-difference scheme achieves its optimal accuracy at $h = (3.078 \pm 0.001) \times 10^{-3}$ and produces a numerical error of $(1.148 \pm 0.6) \times 10^{-11}$. This error is roughly two orders of magnitude smaller than that of the second–order method. Although the sixth–order approximation reduces the error by an additional factor of ten, it causes a substantially higher computational cost.

In Variational Monte Carlo (VMC) calculations, a numerical error of 10^{-11} already lies far below the intrinsic statistical uncertainty of the Monte Carlo estimator. Reducing the truncation error further offers little practical benefit while increasing the computational effort per iteration. I therefore chose the fourth–order method in the finite-difference evaluation of the 3D Laplacian in the calculations.

C. Monte Carlo Verification

I use gradient descent minimisation to find the highest efficient rate $r = 0.2261(9)$ at $\delta = 1.71(7)$ for 1D Metropolis sampling. The acceptance rate is $0.4384(3)$, which agrees with the general tuning result. I then calculated local energy $E_l(x)$ and compared it with the analytical ground-state value of 0.5 given in project script [1].

I verify the local energy at three points, obtaining $E_l(0.001) = 0.5 - 4 \times 10^{-12}$, $E_l(-0.001) = 0.5 - 3 \times 10^{-12}$, and $E_l(0.1) = 0.5 - 1 \times 10^{-11}$. These results show that the numerical evaluation agrees precisely with the analytical value, with errors consistent with the expected accuracy of the fourth-order finite-difference scheme.

The sampled mean local energy is $\langle H \rangle = 0.5 - (8.7 \pm 0.2) \times 10^{-13}$. The statistical uncertainty, on the order of 10^{-14}, does not originate from Monte Carlo fluctuations—since the ground-state local energy is constant—but from numerical roundoff errors in the floating-point evaluation.

IV. The Hydrogen Atom

A. Hamiltonian and Ansatz

In this section, I use a given parametrised ansatz [1]

$$\psi(\mathbf{r}; \theta) = e^{-\theta r}. \tag{10}$$

to find the ground state eigenfunction of the Hydrogen atom under the Born-Oppenheimer approximation. The form of the ansatz preserves spherical symmetry and resembles the exact ground state e^{-r}, allowing a single-parameter optimisation.

I verified the three-dimensional Laplacian by comparing the numerical results with the analytical values of the test function $f(x, y, z) = e^{x^2+y^2+z^2}$ at the point $(1, 1, 1)$. The error is 6×10^{-11}, confirming the accuracy of the finite-difference Laplacian.

B. 3D Metropolis Sampling

Using the same gradient-descent procedure, I obtained an optimal proposal step size of $\delta = 1.05(4)$, which corresponds to an efficiency ratio of $r = 0.051(1)$. This choice of δ yields an acceptance rate of approximately $0.3810(7)$.

C. Gradient of Energy and Minimisation

The gradient of the variational energy with respect to θ is evaluated using

$$\partial_\theta \langle H \rangle \approx \frac{2}{N_s} \sum_{i=1}^{N_s} \left[\big(E_l(\mathbf{R}^{(i)}) - \langle H \rangle \big) \frac{\partial_\theta \psi(\mathbf{R}^{(i)}; \theta)}{\psi(\mathbf{R}^{(i)}; \theta)} \right] \tag{11}$$

where the configurations $\mathbf{R}^{(i)}$ are drawn from the Metropolis sampler according to $\rho(\mathbf{R}; \theta)$. In this situation, the variational Monte Carlo only has one parameter. Therefore I choose a 1D gradient descent minimization method to find the optimal value of $\theta = (9.999946 \pm 0.000001) \times 10^{-1}$. Fixing θ at 0.9999946, the ground-state energy is $\langle H \rangle = -0.4997 \pm 0.0001$, and this recomputation is

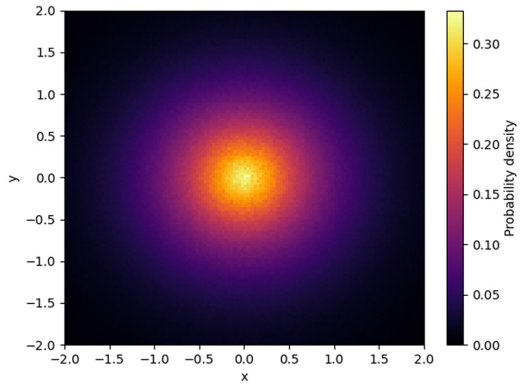

Fig. 4: Projected probability density of the hydrogen atom ground state onto the x–y plane, obtained from Metropolis sampling. Higher density near the origin reflects the expected exponential localization of the ground-state orbital.

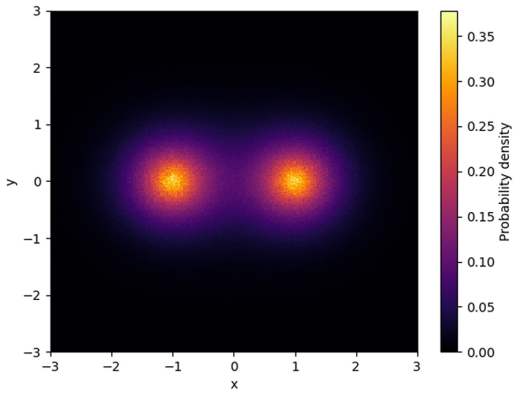

Fig. 5: Projected probability density of the H_2 ground-state wavefunction onto the x–y plane for an internuclear separation of $r = 2$ bohr. The two density maxima correspond to the positions of the nuclei, illustrating the expected bonding structure.

required to obtain an unbiased energy estimate free from the parameter-updating noise present during optimization. The histogram plot of x-y plane is shown in Fig. 4.

V. The Hydrogen Molecule H_2

A. Hamiltonian and Two-Electron Ansatz

To obtain the ground-state eigenfunction of the hydrogen molecule, I employ a parametrized ansatz with three variational parameters θ_i $(i = 1, 2, 3)$ [1]:

$$\psi(\mathbf{r}_1, \mathbf{r}_2, \boldsymbol{\theta}) = \left[e^{-\theta_1(|\mathbf{r}_1-\mathbf{q}_1|+|\mathbf{r}_2-\mathbf{q}_2|)} + e^{-\theta_1(|\mathbf{r}_1-\mathbf{q}_2|+|\mathbf{r}_2-\mathbf{q}_1|)}\right] \times \exp\left[\frac{-\theta_2}{1+\theta_3 r_{12}}\right], \tag{12}$$

where $r_{12} = |\mathbf{r}_1 - \mathbf{r}_2|$ is the inter-electronic separation, $\mathbf{r}_1$ and $\mathbf{r}_2$ denote the electron positions, and $|\mathbf{q}_1 - \mathbf{q}_2|$ is the atomic distance.

B. 6D Metropolis Sampling

The six-dimensional Metropolis sampler was validated using a standard six-dimensional Gaussian test distribution. From this benchmark, the optimal proposal step size was determined to be $\delta = 0.75(4)$, with an efficiency of $r = 0.027(2)$. The corresponding acceptance rate, $0.3945(7)$, is consistent with the expected behaviour of Metropolis algorithms in higher-dimensional spaces. A two-dimensional histogram of the sampled probability distribution at an atomic distance of $r = 2$ is shown in Fig. 5.

C. Energy Minimisation

Guided by preliminary minimization results, the initial parameter vector was chosen as $\boldsymbol{\theta}_0 = (1.55, 0.355, 0.55)$, which provides a favourable starting point and leads to faster convergence in practice. For an internuclear separation of $r = 2$, the minimum expectation value of the Hamiltonian is obtained as $\langle H \rangle = -1.101(5)$ at the optimal parameters $\boldsymbol{\theta}_{\text{opt}} = (1.054, 0.352, 0.550)$. Since both $\boldsymbol{\theta}_{\text{opt}}$ and the corresponding minimum energy vary with r, the Quasi-Newton procedure is applied across a range of internuclear separations to generate the data required for fitting the Morse potential.

VI. Fitting to the Morse Potential

Given energies $E(r)$ at various atomic distances r, I use χ^2 minimization to fit for the Morse potential [1]

$$V_{\text{Morse}}(r) = D(1 - e^{-a(r-r_0)})^2 - D + 2E_{\text{single}}. \tag{13}$$

where $E_{\text{single}} = -0.4997 \pm 0.0001$ Hartree.

An initial grid scan using 20 points over the range $r \in [0.5, 5]$ was performed to identify the overall shape of the Morse potential. To better resolve the behaviour near the minimum, the range was subsequently restricted to $r \in [1, 3]$. The minimum is found to occur near $r = 1.4$ bohr, and additional sampling points were generated in the interval $r \in [1, 2]$ to improve the fit in this region. The resulting fitted Morse potential is shown in Fig. 6.

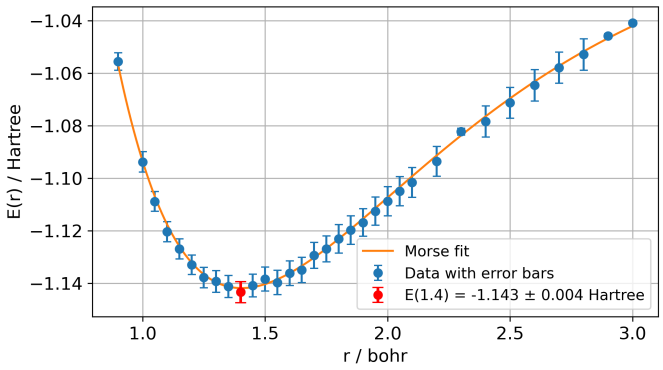

Fig. 6: Morse potential fit to the variational Monte Carlo energies of H_2 as a function of internuclear separation r. The blue data points show a local minimum near $r = 1.4$ bohr, highlighted by the red marker, while the orange curve represents the χ^2 fit of Eq. 13.

VII. Results and Discussion

The fitted Morse potential parameters are

$$r_0 = 1.404 \pm 0.001 \text{ bohr},$$
$$D = 0.1425 \pm 0.0003 \text{ Hartree},$$
$$a = 1.136 \pm 0.005 \text{ bohr}^{-1}.$$

Physically, r_0 corresponds to the equilibrium bond length, D to the dissociation energy, and a to the bond stiffness near equilibrium. The fitted value $r_0 \approx 1.4$ bohr is close to experiment, indicating that the variational ansatz captures the essential features of covalent bonding in H_2 [1]. The dissociation energy is underestimated relative to the reference value of ~ 0.17 Hartree, reflecting limitations of the three-parameter ansatz, the approximate Morse form, and the fixed-nuclei approximation, which neglects vibrational zero-point effects [4], [5].

The statistical consistency of the VMC energies and fitted Morse parameters is validated by examining the Monte Carlo uncertainties. Each energy point has a statistical error of $\sigma_E \sim 0.004$ Hartree. With $N_s = 10^6$ samples and an efficiency $r = 0.027$, the effective sample size is $N_{\text{eff}} \approx 2.7 \times 10^4$, implying local-energy fluctuations of $\sigma_{E_L} \sim 0.7$ Hartree via $\sigma_{\langle H \rangle} \approx \sigma_{E_L}/\sqrt{N_{\text{eff}}}$. Such fluctuations arise from the use of an approximate trial wavefunction; for an exact eigenstate, the local energy would be constant [5].

In the Morse fit, the dissociation energy D is primarily constrained by the vertical energy scale. Since $\partial E/\partial D = -1$ at $r = r_0$ and D is inferred from $N = 32$ data points, its uncertainty is estimated as $\sigma_E/\sqrt{N} \approx 7 \times 10^{-4}$ Hartree, consistent with the fitted error of order 3×10^{-4} Hartree. The parameters r_0 and a, while not determined by a single local sensitivity, exhibit uncertainties of comparable magnitude through standard error propagation in the fit.

VIII. Conclusion

This project implemented a complete Variational Monte Carlo (VMC) workflow for hydrogenic systems, yielding accurate ground-state energies for both the hydrogen atom and molecule. The numerical differentiation, Metropolis sampling, and stochastic optimization methods were validated, and the three-parameter ansatz produced physically meaningful Morse potential parameters consistent with known values.

Challenges included autocorrelation in Metropolis sampling and the increased complexity of multi-parameter optimization for H_2, although the Quasi-Newton method remained robust under Monte Carlo noise. A natural extension of this work would be to use correlated sampling when comparing nearby parameter values, which could reduce variance in energy differences and lead to more stable gradients during optimisation.

Acknowledgment

I acknowledge the use of ChatGPT-5 (OpenAI, https://chatgpt.com) to help me summarize references and debug the code. I confirm that no content directly generated by AI has been presented as my own work.

References

[1] M. Scott and J. Owen, "Project 3: Variational quantum monte carlo," https://bb.imperial.ac.uk/ultra/courses/_45818_1/cl/outline, 2025, computational Physics 2025–26 course handout, Imperial College London.

[2] T. Homem-de Mello and G. Bayraksan, "Monte carlo sampling-based methods for stochastic optimization," *Surveys in Operations Research and Management Science*, vol. 19, no. 1, pp. 56–85, 2014.

[3] W. Janke, "Monte carlo methods in classical statistical physics," in *Computational many-particle physics*. Springer, 2008.

[4] B. L. Hammond, W. A. Lester, and P. J. Reynolds, *Monte Carlo methods in ab initio quantum chemistry*. World Scientific, 1994, vol. 1.

[5] W. M. Foulkes, L. Mitas, R. Needs, and G. Rajagopal, "Quantum monte carlo simulations of solids," *Reviews of Modern Physics*, vol. 73, no. 1, p. 33, 2001.